Monthly Notices of the ROYAL ASTRONOMICAL SOCIETY

MNRAS **00,** 1–10 (2024) https://doi.org/10.1093/mnras/stae591

The escape of fast radio burst emission from magnetars

Maxim Lyutikov ★

Department of Physics and Astronomy, Purdue University, 525 Northwestern Avenue, West Lafayette, IN 47907-2036, USA

Accepted 2024 February 13. Received 2024 February 8; in original form 2023 October 4

ABSTRACT

We reconsider the escape of high-brightness coherent emission of fast radio bursts (FRBs) from magnetars' magnetospheres, and conclude that there are numerous ways for the powerful FRB pulse to avoid non-linear absorption. Sufficiently strong surface magnetic fields, ≥ 10 per cent of the quantum field, limit the waves' non-linearity to moderate values. For weaker fields, the electric field experienced by a particle is limited by a combined ponderomotive and parallel-adiabatic forward acceleration of charges by the incoming FRB pulse along the magnetic field lines newly opened during FRB/coronal mass ejection. As a result, particles surf the weaker front part of the pulse, experiencing low radiative losses, and are cleared from the magnetosphere for the bulk of the pulse to propagate. We also find that initial mildly relativistic radial plasma flow further reduces losses.

Key words: stars: magnetars – fast radio bursts.

1 INTRODUCTION

Observations of correlated radio and X-ray bursts (Bochenek et al. 2020; CHIME/FRB Collaboration 2020; Mereghetti et al. 2020; Li et al. 2021; Ridnaia et al. 2021) established the fast radio burst (FRB)–magnetar connection. There is a long list of arguments in favour of magnetospheric *loci* of FRBs (e.g. Lyutikov 2003; Popov & Postnov 2013; Lyutikov, Burzawa & Popov 2016; Lyutikov & Popov 2020), as opposed e.g. to the wind (e.g. Lyubarsky 2014; Beloborodov 2017; Metzger, Margalit & Sironi 2019; Thompson 2022) [see also reconsideration of wind dynamics by Sharma, Barkov & Lyutikov (2023), arguing against appearance of shocks]. For example, temporal coincidence between the radio and X-ray profiles, down to milliseconds, is a strong argument in favour of magnetospheric origin (Lyutikov & Popov 2020): we know that X-rays are magnetospheric events, as demonstrated by the periodic oscillations seen in giant flares (Hurley et al. 2005; Palmer et al. 2005).

In fact, strong magnetic fields are needed in the emission region to suppress strong 'normal' (non-coherent) losses in magnetar magnetospheres. In the absence of strong guide field, a coherently emitting particle will lose energy on time-scales shorter than the coherent low-frequency wave (Lyutikov, Burzawa & Popov 2016; Lyutikov & Rafat 2019). It is required that the cyclotron frequency be much larger than the wave frequency in the emission region. This requirement limits emission regions to the magnetospheres of neutron stars.

A somewhat separate issue is the escape of the powerful radio waves from the magnetosphere: as the waves propagate in the (presumably) dipole magnetosphere, their amplitude decreases slower than that of the guide field. Beloborodov (2021, 2022, 2023) argued that strong electromagnetic wave, even if generated with the magnetars' magnetospheres, would not escape. The argument, in the simplest form, goes as follows: when the electromagnetic field becomes larger than the guide field, for some waves, for which there is a component of the wave's magnetic field along the guide field, there are periodic instances when electric field becomes larger than the magnetic field. This leads to efficient particle acceleration and dissipation of the wave's energy. Along similar line of reasoning, Golbraikh & Lyubarsky (2023) argued that the non-linear decay of the fast magnetosonic into the Alfvén waves would lead to efficient energy dissipation of the wave.

Here, we argue that the particular case considered in Beloborodov (2021, 2022, 2023) is extreme, not indicative of the more general situation (see also Qu, Kumar & Zhang 2022). Most importantly, ponderomotive acceleration results in a very slow rate of overtaking the particle by the wave – particles surf the weaker ramp-up part of the pulse for a long time, experiencing mild local intensity of the wave, and radiative losses much smaller than those in the fully developed pulse.

Several other related issues are geometry of the magnetic field and wave polarization: Beloborodov (2021, 2022, 2023) considered X-mode (when the magnetic field of the wave adds/subtracts from the guide field) propagating nearly perpendicularly with respect to the guide field (e.g. strictly equatorial propagation considered in Beloborodov 2023) – this is the most dissipative case.

2 NON-LINEAR WAVES WITH GUIDE FIELD

2.1 Basic parameters

There are several important parameters for non-linear wave–particle interaction. First, there is the laser non-linearity parameter (Akhiezer et al. 1975)

$$a_0 \equiv \frac{eE_{\rm w}}{m_e c\omega}, \tag{1}$$

★ E-mail: lyutikov@purdue.edu

where $E_w = B_w$ is the electric field in the coherent wave and ω is the frequency (parameter a_0 is Lorentz invariant). In the absence of guide field, the non-linearity parameter (1) is of the order of a dimensionless momentum of transverse motion of a particle in the EM wave, in the frame where particle is on average at rest. In this case (no guide field), for $a_0 \geq 1$ the particle motion becomes relativistic. The transverse Lorentz factor, as measured in the gyration frame, is $\gamma_0 = \sqrt{1+a_0^2}$ (for circularly polarized waves; $\gamma_0 = \sqrt{1+a_0^2/2}$ for linearly polarized wave).

The second important parameter is the relative amplitude of the electromagnetic field of the wave with respect to the guide field:

$$\delta = \frac{B_w}{B_0}. \tag{2}$$

Then, there is the ratio of the cyclotron frequency to wave frequency:

$$f = \frac{\omega_B}{\omega}. \tag{3}$$

The three parameters combine as follows:

$$a_0 = \delta f. \tag{4}$$

The corresponding combination on the right-hand side is Lorentz invariant under a boost along the guide magnetic field.

It turns out (see equation 30) that another important combination is

$$\tilde{a}_0 = \frac{a_0}{1+f}. \tag{5}$$

This is effective non-linearity parameter for non-linear electromagnetic wave in finite guide field (parameter f is defined in the lab frame, where initially a particle is at rest).

2.2 FRBs' parameters

For fiducial estimates, consider an FRB pulse coming from $d = $ Gpc, of duration $\tau = 1$ ms, and producing flux $F_\nu = 1$ Jy at frequency of $\nu = 10^9$ Hz (these values are at the higher end of the FRB parameters). The isotropic equivalent luminosity and total energy (in radio) are then

$$\begin{aligned} L_{\rm iso} &= 4\pi D^2 \nu F_\nu = 10^{42}\, {\rm erg\, s^{-1}}, \\ E_{\rm iso} &= L_{\rm iso}\tau = 10^{39}\, {\rm erg}. \end{aligned} \tag{6}$$

The electromagnetic field of the wave at distance r from the source is

$$B_w = \frac{2\sqrt{\pi}\sqrt{\nu F_\nu}\, d}{\sqrt{c}\, r} = 6\times 10^9 \left(\frac{r}{R_{\rm NS}}\right)^{-1} {\rm G}. \tag{7}$$

The laser non-linearity parameter a_0^* at the surface of the neutron star then evaluates to

$$a_0^* = \frac{e\sqrt{F_\nu}\, d}{\sqrt{\pi} m_e c^{3/2} \nu^{1/2} R_{\rm NS}} = 10^7. \tag{8}$$

If we normalize the surface magnetic field to the quantum field

$$\begin{aligned} B_{\rm NS} &= b_{\rm q} B_{\rm Q} \\ B_{\rm Q} &= \frac{c^3 m_e^2}{e\hbar} \end{aligned} \tag{9}$$

and for now assume dipolar field

$$\begin{aligned} B_0 &= B_{\rm NS}(r/R_{\rm NS})^{-3}, \\ a_0 &= a_0^*(r/R_{\rm NS})^{-1}, \end{aligned} \tag{10}$$

then the relative amplitude of the fluctuating field and the ratio of frequencies are

$$\begin{aligned} \delta &= \frac{B_w}{B_0} = \frac{2\sqrt{\pi} d \sqrt{\nu F_\nu} r^2}{\sqrt{c} B_{\rm NS} R_{\rm NS}} = 10^{-4} b_{\rm q}^{-1} \left(\frac{r}{R_{\rm NS}}\right)^2, \\ f &= b_{\rm q} \frac{e B_{\rm Q}}{2\pi m_e c \nu} \left(\frac{r}{R_{\rm NS}}\right)^{-3} = 10^{11} b_{\rm q} \left(\frac{r}{R_{\rm NS}}\right)^{-3}, \end{aligned} \tag{11}$$

see Fig. 1.

The amplitude of electromagnetic fluctuations in the wave becomes comparable to the guide field ($\delta \sim 1$) at

$$\frac{r_0}{R_{\rm NS}} \approx 10^2 b_{\rm q}^{1/2}. \tag{12}$$

At that point

$$\begin{aligned} &a_0[r_0] \approx 2\times 10^5, \\ &f(r_0) = a_0[r_0] = 2\times 10^5. \end{aligned} \tag{13}$$

The wave's frequency equals cyclotron frequency at

$$\begin{aligned} &\frac{r_f}{r_0} = a_0[r_0]^{1/3}, \\ &\frac{r_f}{R_{\rm NS}} \approx 5\times 10^3 b_{\rm q}^{1/3}, \\ &a_0(r_f) = a_0[r_0]^{2/3}. \end{aligned} \tag{14}$$

The key parameter $\tilde{a}_0$, equation (5), has a maximum (for dipole field) at

$$\begin{aligned} &r/r_0 = (2a_0[r_0])^{1/3} = 2^{1/3} r_f, \\ &\tilde{a}_0^{(\max)} = \frac{2^{2/3}}{3} a_0[r_0]^{2/3}. \end{aligned} \tag{15}$$

This estimates to

$$\begin{aligned} \left(\frac{r}{R_{\rm NS}}\right) &= b_{\rm q}^{1/3} \left(\frac{c^2 m_e}{\pi\hbar\nu}\right)^{1/3} = 6\times 10^3 \times b_{\rm q}^{1/3}, \\ \tilde{a}_0^{(\max)} &\approx 1.8\times 10^3 \times b_{\rm q}^{-1/3}. \end{aligned} \tag{16}$$

Parameter $\tilde{a}_0^{(\max)}$, equation (16) is an important one. This is an estimate of the maximal total Lorentz factor, $\sim \tilde{a}_0^{(max),2}$, maximal parallel Lorentz factor, $\sim \tilde{a}_0^{(\max)}$, and maximal transverse momentum $\sim \tilde{a}_0^{(\max)}$.

For example, maximal values of the Lorentz factor are achieved at $r/r_0 = (2a_0[r_0])^{1/3}$ and equals

$$\gamma_p = 1 + \frac{2^{1/3}}{9} a_0[r_0]^{4/3}. \tag{17}$$

These values are large, and in the magnetospheres of magnetars would lead to large radiative losses, killing the EM pulse. We argue that these high values are not reached.

For the maximal $\tilde{a}_0^{(\max)}$ to be reached with the magnetosphere, the period should be sufficiently long $P \geq 1$ s. For shorter periods, the value of $\tilde{a}_0^{(\max)}$ is reached at the light cylinder (see Fig. 2). For mildly magnetized neutron stars, with regular surface field $\sim 10^{12}$ G ($b_{\rm q} = 0.02$), spinning with period $P \sim 20$ ms, the value of $\tilde{a}_0^{(\max)}$ can reach nearly 10^4. It is not clear why FRB sources would fall into this special regime: higher surface field and faster spins push $\tilde{a}_0^{(\max)}$ towards smaller values. For example, for quantum surface field $b_{\rm q} = 1$ and period of 10 ms, $\tilde{a}_0^{(\max)}$ is tiny, ≤ 1.

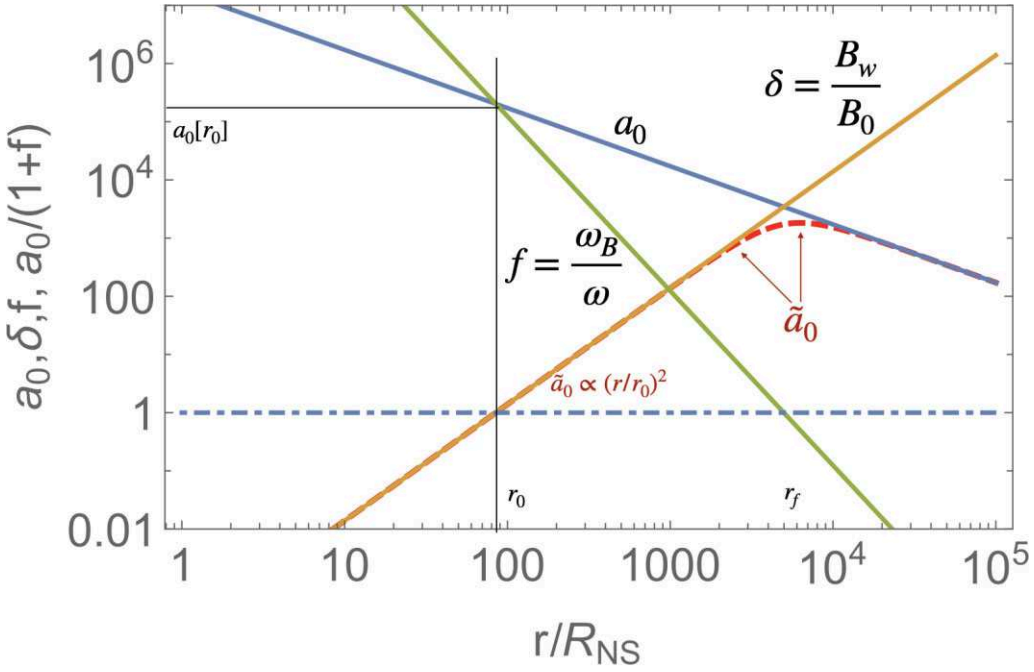

Figure 1. Evolution of basic parameters in the dipolar magnetosphere: non-linearity parameter a_0, relative wave intensity $\delta = B_w/B_0$, ratio of frequencies $f = \omega_B/\omega$, and effective non-linearity parameter $\tilde{a}_0 = a_0/(1+f)$. Indicated are radii r_0 (where $\tilde{a}_0 = 1$), value of $a_0[r_0]$, and radius r_f, where $f = 1$. Maximal value of $\tilde{a}_0^{(\max)} \approx 1.8 \times 10^3$ is reached approximately at r_f.

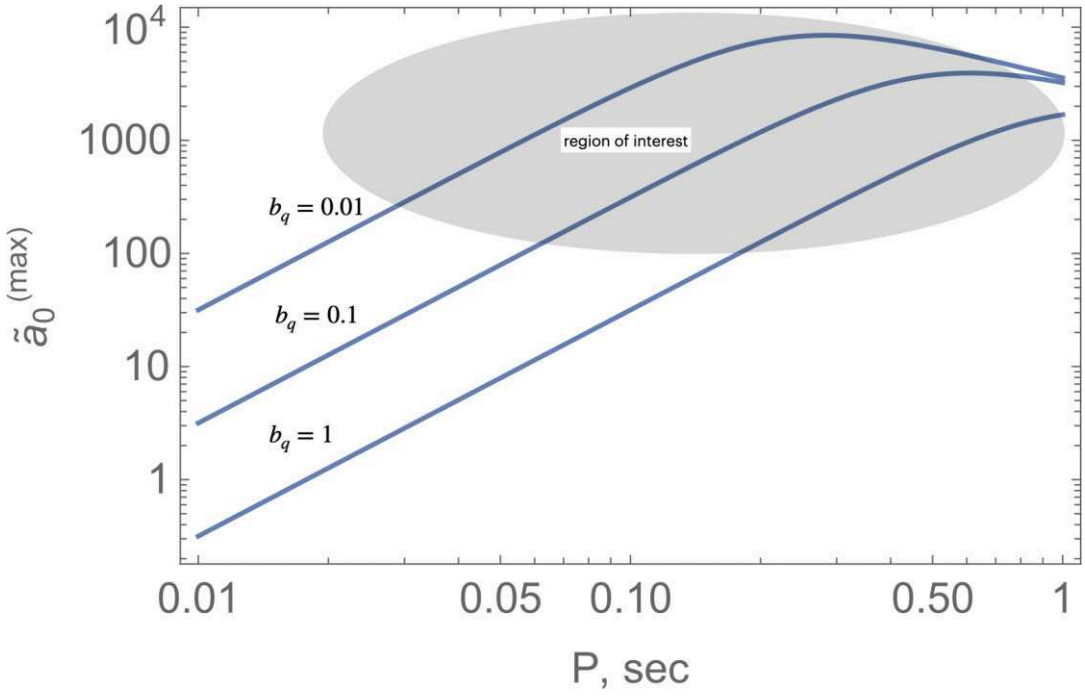

Figure 2. Maximal values of the non-linearity parameter $\tilde{a}_0$ reached at the light cylinder for spins faster than $P = 1$ s (for slower spins see equation 16), as function of the surface field $b_q = B_{NS}/B_Q$. Smaller magnetic fields are less efficient in suppressing $\tilde{a}_0$. 'Region of interest' indicates a set of parameters when wave's non-linearity may become large, ≥ 100.

2.3 Post-eruption magnetic field lines are mostly radial, magnetic field increases in the outer parts of the magnetosphere

There are, qualitatively, three energy sources during FRB/magnetospheric eruption: (i) dynamical magnetic field; (ii) high-energy emission; (iii) radio emission. Energetically, (i) $\gg$ (ii) $\gg$ (iii), so that the dominant effects to the distortion of the magnetic field come not from radiation, but from magnetospheric dynamics during the eruption.

The dynamical magnetic field is produced by a process that initiates magnetospheric eruption, *e.g.*, in an analogue to solar

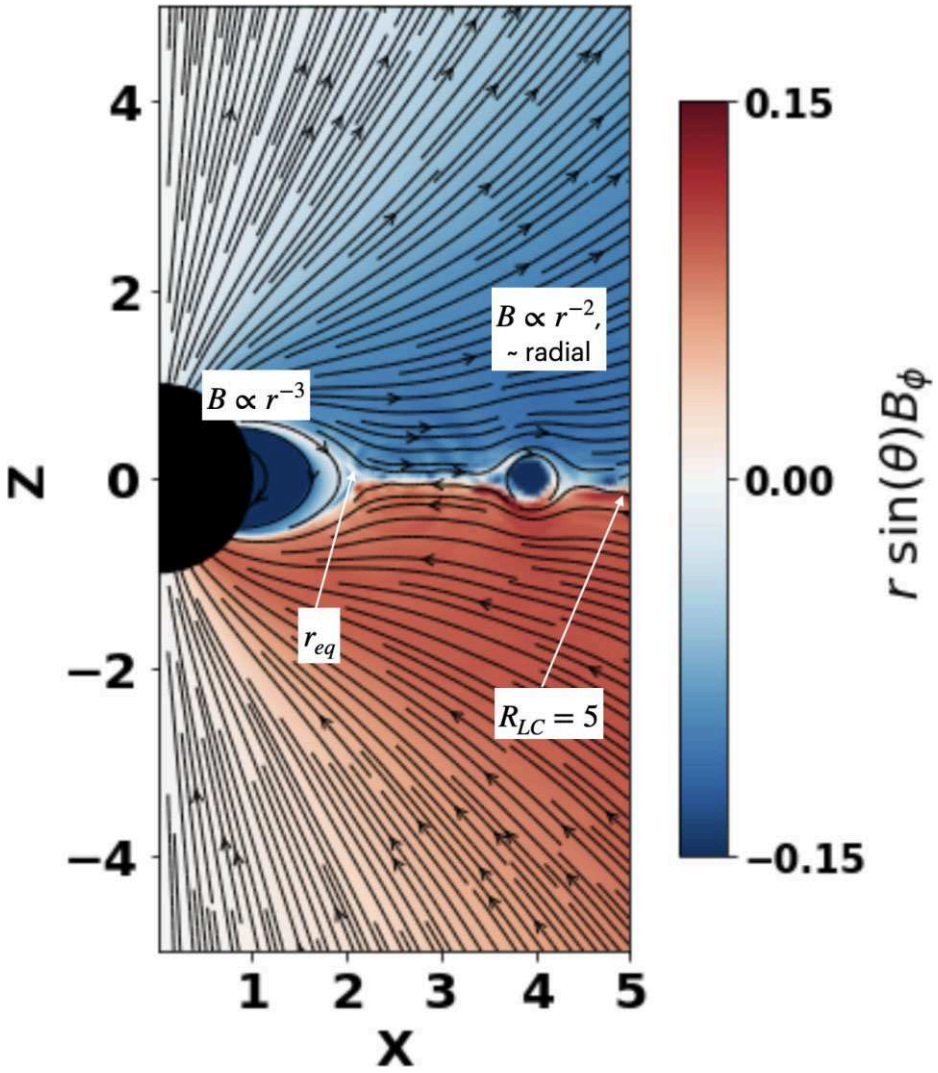

Figure 3. Post-flare opening of the magnetosphere (Sharma, Barkov & Lyutikov 2023). Colour is values $r\sin\theta B_\phi$, lines are poloidal field line. The spin parameter is $\Omega = 0.2$, so that the light cylinder is at $R_{\rm LC} = 5$. Post-flare magnetosphere is open starting $r_{\rm eq} \ll R_{\rm LC}$ (20). Beyond $r_{\rm eq}$, the magnetosphere has monopolar-like magnetic field structure.

coronal mass ejection (CME). During CME, a topologically isolated structure is injected into the magnetosphere (Lyutikov 2022; Sharma, Barkov & Lyutikov 2023). Let us assume that injection (generation of topologically disconnected magnetic structure) occurs near the stellar surface with the typical size $R_{\rm CME,0} \leq R_{\rm NS}$ and associated energy $E_{\rm CME,0}$. An important parameter is the total magnetic energy of the magnetosphere,

$$E_{B,\rm NS} \sim B_0^2 R_{\rm NS}^3. \tag{18}$$

Naturally, the injected energy is much smaller than the total energy,

$$\eta_{\rm CME} = \frac{E_{\rm CME,0}}{E_{B,\rm NS}} \leq 1. \tag{19}$$

As the CME is breaking-out through the overlaying magnetic field, it does work on the magnetospheric magnetic field. At some point, 'detonation' occurs: when the total energy contained in the confining magnetic field exterior to the position of the CME ($\sim B_0^2 R_{\rm NS}^6 r^{-3}$) becomes smaller than the CME's internal energy (equivalently, when the size of the CME becomes comparable to the distance to the star). This occurs at some equipartition radius $r_{\rm eq}$:

$$\frac{r_{\rm eq}}{R_{\rm NS}} \sim \frac{E_{B,\rm NS}}{E_{\rm CME,0}} = \eta_{\rm CME}^{-1} \geq 1. \tag{20}$$

Immediately after the generation of a CME the magnetosphere becomes open, with nearly radial magnetic field lines for $r \geq r_{\rm eq}$.

For quantum surface field $E_{B,\rm NS} \sim 2 \times 10^{45}$ erg. The injected energy $E_{\rm CME,0}$ is hard to estimate: the observed radio energy is an absolute lower limit. Much more energy is radiated in X-rays, even more is contained in the fields. (Also CME is losing energy to pdV work as it breaks through the overlaying magnetic field; Lyutikov 2022; Sharma, Barkov & Lyutikov 2023). It is conceivable that the relative injected energy may reach $\sim$ per cent level of the total energy, $\eta_{\rm CME} \sim 10^{-2}$. In this case, since beyond $r_{\rm eq}$ the magnetic field decreases slower than dipole, $B \propto r^{-2}$ instead of $B \propto r^{-3}$, the region where $f = \omega_B/\omega \geq 1$ will extend further. (Larger guide field suppresses particle's transverse motion, see Fig. 4.)

Most importantly, beyond $r_{\rm eq}$ the magnetic field becomes mostly radial, Fig. 3. As a result, the electromagnetic waves generated close to the neutron star surface propagate nearly along the local field line.

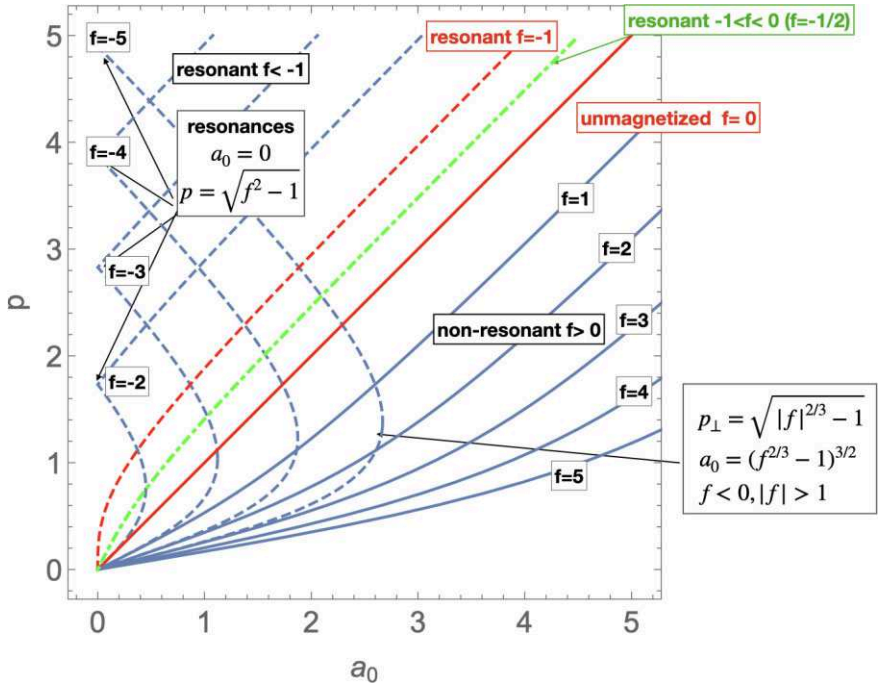

Figure 4. Particle's transverse momenta in strong circularly polarized electromagnetic wave in external magnetic field. Wave intensity is parametrized by laser parameter a_0. Different curves correspond to different $f = \pm\omega_B/\omega$ (different charges or polarizations).

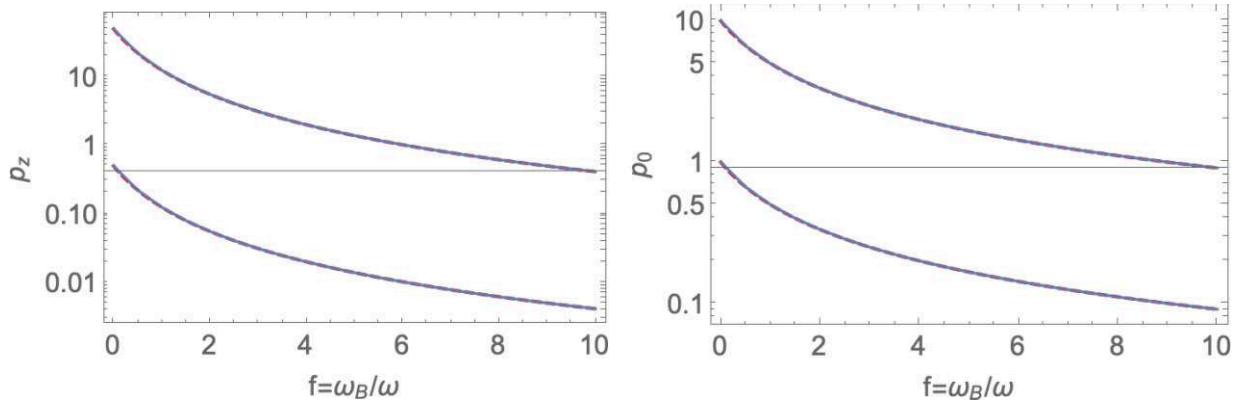

Figure 5. Ponderomotive acceleration by a circularly polarized electromagnetic pulse propagating along the guide field, non resonant case $f > 0$. Plotted is the axial momentum p_z (left panel) and transverse momentum p_0 (right panel) as a function of $f = \omega_B/\omega$ (ω defined in the lab frame) for two cases: $a_0 = 1$ (bottom curves) and $a_0 = 10$ (top curves). Dashed line is analytical result, equation (30). Numerical and analytical curves nearly coincide. These plots serves to illustrate the numerical precision of the code, and to validate the analytics.

As we demonstrate in this work, this case does not suffer from strong radiative.

Finally, plasma is likely to stream out along the open field lines even before the FRB wave comes – this further freezes out wave–particle interaction.

3 PARTICLE DYNAMICS IN CIRCULARLY POLARIZED WAVE PROPAGATING ALONG GUIDE FIELD

3.1 Beam frame

Circularly polarized waves allow for exact analytical solutions, and thus provide benchmark for simulations and guidance for the more complicated linearly polarized case.

In the beam frame (beam frame is defined as a frame where average parallel momentum of ponderomotively accelerated particles is zero) a force balance for a particle moving in electromagnetic field and guide magnetic field reads

$$d_t\mathbf{p} = e\left(\mathbf{E}_w + \mathbf{p}\times(\mathbf{B}_0 + \mathbf{B}_w)/\gamma\right) \;\rightarrow\; \gamma_\pm m_e v_\pm \omega = e(E_w \pm v_\pm B_0), \tag{21}$$

where all quantities are positive: $\pm$ accounts for two directions of the background field/charge/polarization sign (speed of light is set to unity). Relations describe a charge which velocity at each moment (counter)-aligns with the magnetic field in the wave (Zeldovich 1975). For a more general case, see Roberts & Buchsbaum (1964) and Kong & Liu (2007).

In dimensionless notations, the motion of a particle in circularly polarized electromagnetic wave obeys

$$a_0 = p_0 \left| 1 + \frac{1}{\sqrt{1+p_0^2}} f \right|,$$
$$\gamma_0 = \frac{1}{\sqrt{1-v_0^2}}, \tag{22}$$

(here, ω is the wave frequency in the beam frame and v_0, p_0 are corresponding velocity/momenta), see Fig. 4. Quantity f can be negative: two signs correspond to two polarizations (or two signs of charges). Absolute value $|...|$ ensures the definition of $a_0 \geq 0$; crossing the resonant condition for the minus sign changes just the phases of the particles. Below in this section, we drop the prime, with clear understanding that the quantities are measured in the plasma frame.

In (22), the values for γ_0 (for given a_0 and $|f|$) are different for two charges, especially near the cyclotron resonance $f \approx -1$. As we are not considering here the effects of cyclotron absorption, we assume below that $-f$ is not too close to unity.

In the case of strong electromagnetic pulse with $a_0 \gg 1$, there are qualitatively three regimes: (i) small guide field $f \ll 1$, $p_0 \sim a_0$; (ii) medium guide field $1 \ll f \ll a_0$, $p_0 \approx \delta \gg 1$ (in this case the transverse motion is still relativistic: a wave is sufficiently strong so that it accelerate particles to relativistic motion on time-scale of $1/\omega_B$; (iii) dominant guide field $f \gg a_0$, $v_0 \sim \delta \ll 1$ (in this case a particle just experiences E-cross-B drift).

3.2 Ponderomotive acceleration by circularly polarized wave propagating along the guide field

The above discussion in Section 3.1 omits the most important issue: the ponderomotive effects – how incoming wave modifies the properties of the plasma. As this is the most important part of the work, we give here detailed derivations.

Let a transverse circularly polarized wave of given strength E_w, frequency ω (measured in lab frame), non-linearity parameter a_0, propagating along guide magnetic field $B_0 \mathbf{e}_z$. Noting that

$$\partial_t \gamma = \frac{e}{m_e c^2} \mathbf{E} \cdot \mathbf{v},$$
$$\partial_t p_z = \frac{e}{c} \mathbf{v} \times \mathbf{B}_w|_z, \tag{23}$$

and expressing fields in terms of the vector potential

$$\mathbf{E}_w = -\partial_t \mathbf{A},$$
$$\mathbf{B}_w = \mathrm{curl}\, \mathbf{A}, \tag{24}$$

we find

$$\partial_t \gamma = -v_x \partial_t A_x - v_y \partial_t A_y,$$
$$\partial_t p_z = v_x \partial_z A_x + v_y \partial_z A_y. \tag{25}$$

Thus, the guide field does not enter the relations. Since $A = A(z - t)$, we find then

$$d_t(\gamma - p_z m_e c) = 0. \tag{26}$$

Switching to dimensionless notations and assuming that before the arrival of the wave a particle was at rest, we find

$$\gamma = 1 + p_z. \tag{27}$$

We stress that for circularly polarized wave propagating along the magnetic field, this is valid for arbitrary guide field.

Thus (recall that p_0 is the transverse momentum, hence Lorentz invariant under a boost along z),

$$p_z = \frac{\mathbf{p}_0^2}{2},$$
$$\gamma = 1 + p_0^2/2 = 1 + p_z,$$
$$\gamma_\parallel = \frac{1}{\sqrt{1-\beta_z^2}} = \frac{1 + p_0^2/2}{\sqrt{1+p_0^2}} = \frac{1+p_z}{\sqrt{1+2p_z}},$$
$$\gamma_0 = \sqrt{1+p_0^2},$$
$$\beta_z = \frac{p_0^2}{2+p_0^2},$$
$$\tan\alpha_\mathrm{p} = \frac{p_0}{p_z} = \frac{2}{p_0}, \tag{28}$$

where α_p is pitch angle in lab frame. (Note that $\gamma_\parallel \neq \sqrt{1+p_z^2}$.) These relations establish connection between parallel motion acquired due to ponderomotive force and energy of the particle in the gyration/beam frame for circularly polarized wave, possibly propagating along guide magnetic field.

One remaining step is to connect p_z (or p_0) to the waves' parameters a_0 and f at minus infinity, before interaction with a particle. Using invariance of $a_0 = E_w/\omega$ and ω_B, and Lorentz transformation of the frequency

$$\omega' = (1 - \beta_\parallel)\gamma_\parallel \omega, \tag{29}$$

(where now primes denote quantities measured in the beam frame) we arrive at

$$p_0 = \frac{a_0}{1+f},$$
$$\gamma_\perp = \sqrt{1+p_0^2} = \sqrt{1 + \left(\frac{a_0}{1+f}\right)^2},$$
$$p_z = \frac{a_0^2}{2(1+f)^2},$$
$$\gamma = 1 + \frac{a_0^2}{2(1+f)^2},$$
$$\beta_z = \frac{a_0^2}{2(1+f)^2 + a_0^2},$$
$$\gamma_\parallel = \frac{1}{\sqrt{1-\beta_z^2}} = \frac{a_0^2 + 2(1+f)^2}{2(1+f)\sqrt{a_0^2 + (1+f)^2}} = \frac{\gamma}{\gamma_\perp},$$
$$\tan\alpha = \frac{p_0}{p_z} = \frac{2(1+f)}{a_0}. \tag{30}$$

We observe that the case with guide field is related to the no-guide field if we use

$$\tilde{a}_0 = \frac{a_0}{1+f}. \tag{31}$$

Then relations in magnetic field reduce to the same form as without guide field , see Fig. 5

$$p_0 = \tilde{a}_0,$$
$$p_z = \frac{\tilde{a}_0^2}{2},$$
$$\gamma = 1 + \frac{\tilde{a}_0^2}{2},$$
$$\tan\alpha = \frac{2}{\tilde{a}_0}. \tag{32}$$

Importantly, relations (30)–(32) assume that the system is sufficiently

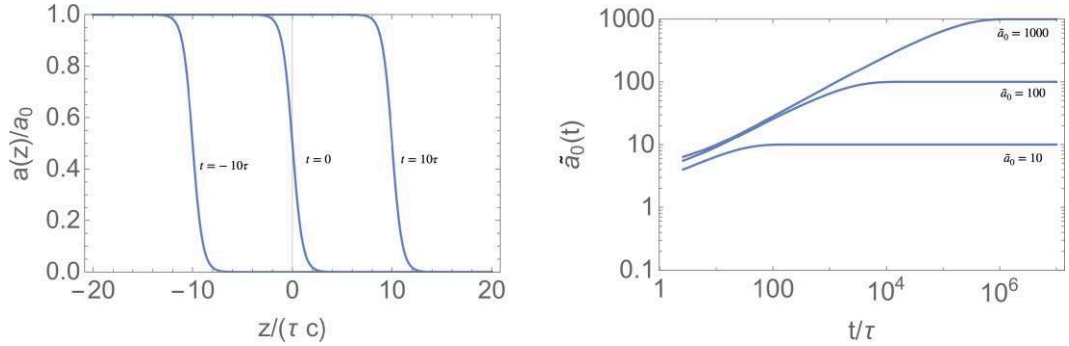

Figure 6. Left panel: An EM pulse with ramp-up width of $\tau = 1$ propagates towards a particle initially at $z = 0$. The pulse ponderomotively accelerates the particle along its direction of propagation. Right panel: Evolution of the non-linearity parameter $\tilde{a}_0(t)$ *at the location of the particles* for $\tilde{a}_0 = 10,\ 100,\ 1000$, constant guide field. Due to ponderomotive acceleration of the particle to $\gamma_\parallel \sim \tilde{a}_0$, the bulk of the pulse reaches the particle after a very long time, $\sim \tilde{a}_0^2\tau$.

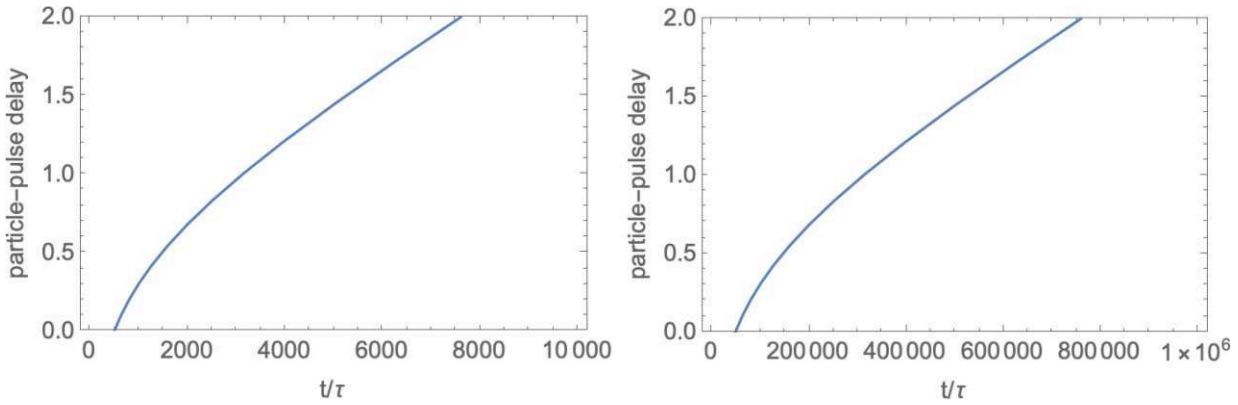

Figure 7. Pulse front – particle delay as function of time [measured in terms of pulse ramp-up time τ for $\tilde{a}_0 = 100$ (left) and $\tilde{a}_0 = 1000$ (right), constant guide field]. The delay becomes of the order of unity after time $\sim (2/5)\tilde{a}_0^2\tau$.

large along the direction of propagation, so that a particle reaches the final steady state. As we show below, this is often not the case in magnetars' magnetospheres.

3.3 Ponderomotive surfing in constant guide field

Ponderomotive force has another important effect: in a system limited in size, the head part of the pulse, which is already non-linear but has local non-linearity parameter much smaller than the pulse, will accelerate a particle to relativistic velocities along wave's direction of propagation, so that it will take a long time for the bulk of the pulse to catch-up with the particle. We consider this effect next.

Consider a wave propagating along the field. Assume that a pulse approaches a particle initially at rest at $z = 0$. The pulse has maximal amplitude a_0 and ramp-up width $\delta z = \tau c$ (Fig. 6). At each moment the axial velocity is

$$\beta_z = \frac{\mathrm{d}z}{\mathrm{d}t} = \frac{\tilde{a}(z)^2}{2 + \tilde{a}(z)^2}. \tag{33}$$

where $\tilde{a}(z)$ is the wave amplitude at the current location of the particle (Fig. 6). Equation (33) can be integrated for $z(t)$ assuming some given profile of the pulse [e.g. $\tanh(z - t)/\tau$].

What is important is not only the absolute value of the intensity $\tilde{a}_0$, but also temporal evolution of the non-linearity parameter *at the location of the particle*, Fig. 6 right panel. Due to ponderomotive acceleration of the particle to $\gamma_\parallel \sim \tilde{a}_0$, the bulk of the pulse reaches the particle after a very long time, $\sim (2/5)\tilde{a}_0^2\tau$.

As another measure, in Fig. 7 we plot a delay between the particle and the centre of the pulse (located at $z = ct$). The delay becomes of the order of the width after time $\sim (2/5)\tilde{a}_0^2\tau$. (The centre of the pulse, where local non-linearity parameter is $\tilde{a}_0/2$ does not even overtake a particle before time $\approx \tau\gamma_0^2/10$.)

3.4 Adiabatic force

The above relations omit an important effect: the adiabatic force that accelerates particles along decreasing magnetic field at the expense of transverse motion.

Adiabatic force can be written as (the parallel component is sometimes called the mirror force Galeev & Sudan 1989)

$$G_\phi = \pm\frac{\beta^2\gamma m_e c^2}{4}\frac{(\mathbf{b}\nabla)B}{B}\sin 2\alpha,$$
$$G_z = \mp\frac{\beta^2\gamma m_e c^2}{2}\frac{(\mathbf{b}\nabla)B}{B}\sin^2\alpha, \tag{34}$$

where $\mathbf{b}$ is unit vector along the magnetic field, α is pitch angle, and upper (lower) signs correspond to particle propagating towards (away from) the regions of increasing magnetic field. Since $\mathbf{G}\cdot\mathbf{v} = 0$, the Lorentz factor γ = constant. Adiabatic force can be thought of as $(\mathbf{m}\cdot\nabla)\mathbf{B}$ force, where $\mathbf{m}$ is the magnetic momentum.

Neglecting particular dependence of the value of the magnetic field on the polar angle,

$$\frac{(\mathbf{b}\nabla)B}{B} = -\frac{1}{3r}, \tag{35}$$

where we chose axis z along the local magnetic field, pointed away from the star, and we assumed that particles are moving away.

In dimensionless notations

$$\partial_t p_\perp = -\frac{\beta^2 \gamma\, p_\perp p_z}{6\left(\gamma^2-1\right) r},$$
$$\partial_t p_z = \frac{\beta^2 \gamma\, p_z^2}{6\left(\gamma^2-1\right) r}. \tag{36}$$

Adiabatic force accelerates along the field at the expense of transverse motion.

To get a feeling of how the adiabatic force affects the dynamics, let us assume that it acts on time-scales longer than pulse ramp-up time. In this case, at each radius there is ponderomotive force, so that total force balance reads

$$\partial_r p_\perp = -\frac{\beta^2 \gamma\, p_\perp p_z}{6\left(\gamma^2-1\right) r} + \partial_r \tilde{a}_0,$$
$$\partial_r p_z = \frac{\beta^2 \gamma\, p_z^2}{6\left(\gamma^2-1\right) r} + \tilde{a}_0 \partial_r \tilde{a}_0. \tag{37}$$

In the region $r_0 \ll r \ll r_f$, $\tilde{a}_0 \approx (r/r_0)^2$. Assuming relativistic motion $\gamma \gg 1$, and $p_z \gg p_\perp$

$$\partial_r p_\perp = -\frac{p_\perp}{6r} + \frac{2r}{r_0^2},$$
$$\partial_r p_z = \frac{p_z}{6r} + \frac{2r^3}{r_0^4}, \tag{38}$$

with solutions

$$p_\perp = \frac{12}{13}\frac{r^2}{r_0^2},$$
$$p_z = \frac{12}{23}\frac{r^4}{r_0^4}. \tag{39}$$

Thus, in the regime of short pulses, with ramp-up scale $\ll r$, the adiabatic force has ~ 10 per cent effect on the particle dynamics, increasing parallel momentum and decreasing the transverse one. Qualitatively, since the losses are high powers of the transverse momentum, this will reduce the losses by about 50 per cent. Our numerical results confirm this conclusion (Fig. 8).

The adiabatic force helps somewhat particles to avoid losses, as it decrease transverse momentum (hence, decreasing radiative losses) and increases parallel momentum (hence, increasing the surfing time).

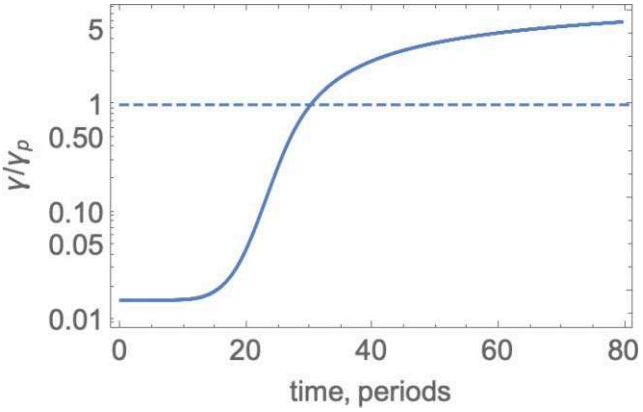

Figure 8. Effect of adiabatic acceleration by Gaussian pulse. Dashed curve: expected maximal Lorentz factor without effects of adiabatic acceleration, equation (17). This illustrates the importance of adiabatic acceleration. Initially, $a_0 = f = 100$, so $\gamma_p = 66$. At time $t = 0$, the peak of the pulse is at -20 wavelengths, rise time is five wavelengths, scale of magnetic field decrease is 10 times the rise time. This confirms that adiabatic effects have about 10 per cent influence on particle dynamics.

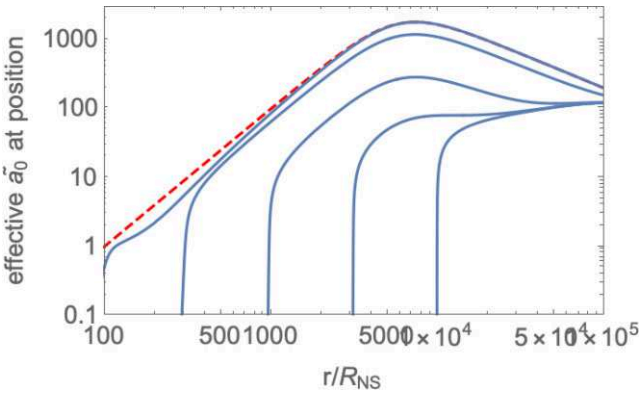

Figure 9. Non-linearity parameter $\tilde{a}_0$ at the location of a particle in dipolar-like magnetosphere for different initial positions of a particle, subject to a pulse $\propto \tanh(r-t)/\tau$ with rump-up time of $\tau = 10 R_{\rm NS}/c$. Red line: local value of $\tilde{a}_0$. This illustrates that particles initially located at $\geq$few r_0 do not experience full waves' non-linearity due to effect of surfing.

4 'GONE WITH THE PULSE'

Above we separately described various ingredients – overall particle dynamics in the beam frame, ponderomotive and adiabatic accelerations. Next, we use these results to study particle dynamics within magnetars' magnetospheres.

4.1 Ponderomotive acceleration in magnetars' magnetospheres

First, we take semi-analytical account of ponderomotive acceleration in magnetars' magnetospheres. We solve equation (33) taking into account both the structure of the pulse and spacial dependence of the parameter $\tilde{a}_0$. The following procedures are applied:

(i) Particle is seeded at a given radius

(ii) An electromagnetic pulse of circularly polarized wave is launched from a much smaller radius. The pulse has a $\propto \tanh(r - t)/\tau$ profile with rump-up time.

(iii) Pulse normalization follows evolution of the parameter $\tilde{a}_0$.

(iv) We numerically integrate equation (33) for the location $z(t)$

In Fig. 9, we show evolution of $\tilde{a}_0$ in the particle frame (as measured at the location of the particle) for different initial positions of the particles. Particles located close to $r_0 = 100 R_{\rm NS}$ initially experience mild parallel acceleration, hence quickly overtaken by the head of the pulse, and find themselves in the strong region of the wave (they do not experience much surfing on the rising part). Particles starting further out quickly gain large Lorentz factors, surf the front part of the pulse, and never experience near-maximal value of $\tilde{a}_0$. Only particles located initially within few r_0 experience maximal wave's intensity.

Qualitatively, in the region $r \geq r_0$ (recall that $r_0 \sim 10^2 R_{\rm NS}$),

$$\tilde{a}_0 \approx \left(\frac{r}{r_0}\right)^2,$$
$$\gamma_\parallel \approx \frac{\tilde{a}_0}{2}. \tag{40}$$

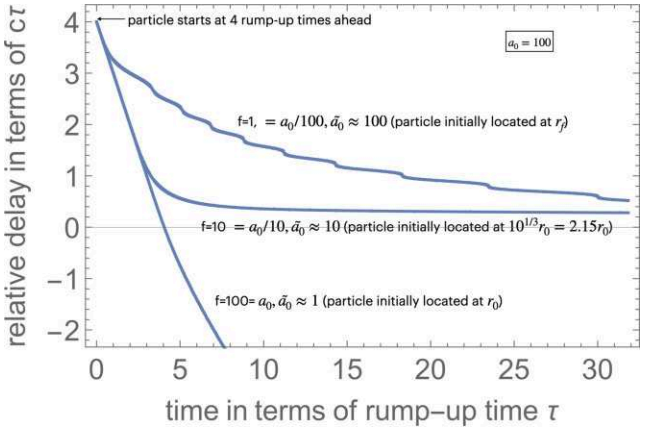

Figure 10. Delay times of 'particle centre of the pulse' for different initial $f = \omega_B/\omega$ parameters (effective different initial locations). Calculations start at four rump-up times, tanh profile the pulse, and magnetic field changes on 10 ramp-up scale.

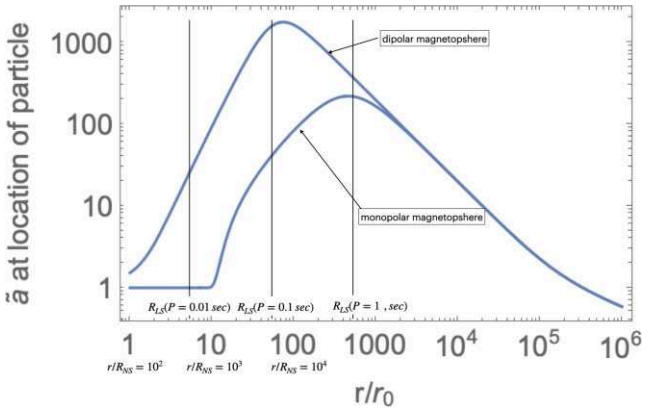

Figure 11. Non-linearity parameter $\tilde{a}_0$ at the location of a particle in dipolar-like and monopolar-like scaling of the guide field. A particle is tracked from the point $r = r_0 = 10^2 R_{\rm NS}$ (equation 12), where $\tilde{a}_0$ first becomes unity. Vertical lines indicate location of the light cylinder for different periods $P = 0.01$, 0.1, and 1 s. The assumed rise time of the FRB pulse is $R_{\rm NS}/c = 30$ μs.

For a pulse with rise time $\tau \sim R_{\rm NS}/c$, the distance $r_{\rm over}$ the pulse would overtake the particle estimates to

$$r_{over} \sim c\tau\gamma_\parallel^2, \tag{41}$$

The condition $r_{\rm over} \sim c/\Omega$ then gives

$$\gamma_\parallel \sim \tilde{a}_0^{(eff)}/2 = (\tau\Omega)^{-1/2} = 70\sqrt{P}, \tag{42}$$

where period P is in seconds. The parameter

$$\tilde{a}_0^{(eff)} \sim 10^2\sqrt{P} \tag{43}$$

is a typical non-linearity parameter that a particle experiences while surfing the pulse. It is an order of magnitude smaller than would be inferred without ponderomotive acceleration (equation 16).

4.2 Ponderomotive and adiabatic acceleration

The above results, integration of the parallel momentum (33), did not take adiabatic acceleration into account. To further clarify the situation, in Fig. 10 numerically integrate particles motion in the field of incoming pulse, in inhomogeneous decreasing guide field. This is done using in-house built Boris-based pusher (Boris & Roberts 1969; Birdsall & Langdon 1991). In the simulations, a particle is initially located four ramp-up scales ahead of the $\tanh(r - t)/\tau$ with rump-up scale $\tau = 5$ wavelength. At the initial location of the particle, the wave intensity corresponds to $\tilde{a}_0 = 100$. Four different parameters, f are shown: $f = 100, 10, 1$. These different values of f mimic different initial locations in the magnetosphere: $f = 100$ corresponds to $r = r_0$, and $f = 1$ corresponds to $r = r_f$. We plot the delay between a local position of a particle and the middle of the pulse, where intensity is half the local maximum.

Our numerical results indicate that combined effects of ponderomotive and adiabatic acceleration hugely increase overtake time. We observe that for $f = 100$ (lower curve, equivalent to starting at $r = r_0$) the head of the pulse quickly passes the particle (since initially its velocity is only mildly relativistic). As a result, a particle quickly 'feels' the full intensity of the wave. In contrast, the head of the pulse never overtakes a particle located midway between r_0 and r_f (middle curve), or further out. This demonstrates that due to a limited radial extent a particle may never reach the terminal state with local $p_0 = \tilde{a}_0$, as predicted by (30).

In all cases, particles initially located beyond r_0 quickly acquire relativistic velocities. For particles near r_0, these relativistic velocities are not sufficient to escape the full non-linearity of the wave, but still, $v \sim c$. Thus, the leading part of the wave will clear particles from the magnetosphere

4.3 Dissipated energy

Let us estimate the expected energy loss by the wave, assuming that the frontal particles lose all the energy, it acquired in the wave. As Fig. 11 indicates, only particles in a narrow layer near r_0 (where $\tilde{a}_0$ just becomes of the order of unity) experience large acceleration. Most of the magnetospheres surf the wave and do reach very large energies. As an estimate of the dissipated power, we can use

(i) volume $V \sim 4\pi r_0^2 \times 3r_0$ (assuming thickness of $3r_0$);

(ii) Lorentz factor $\gamma \sim \left(\tilde{a}_0^{(\max)}\right)^2/2$;

(iii) density $\kappa n_{\rm GJ}$ [$\kappa \sim 10^5$ is multiplicity, and $n_{\rm GJ}$ is the Goldreich & Julian (1970) density];

(iv) period P in seconds.

We find for dissipated energy $E_{\rm dis}$

$$E_{\rm dis} = 5 \times 10^{36} \left(\frac{\kappa}{10^5}\right) P^{-1}\ {\rm erg}, \tag{44}$$

a safely mild value, much smaller than the total energy of the FRB (6).

Fig. 9 also indicates that the bulk of the particles in the magnetosphere experience $\tilde{a}_0 \sim 100$ (hence, $\gamma \sim 5 \times 10^3$). The total associated energy within the light cylinder is then $\sim 5 \times 10^{33}$ erg. Thus, the wave spends most of the energy on cleaning the magnetosphere near $r \sim r_0$.

Finally, in Fig. 11 we plot the non-linearity parameter $\tilde{a}_0$ at the location of a particle in dipolar-like $B \propto r^{-3}$ and monopolar-like $B \propto r^{-2}$ scaling of the guide field. The rise time of the pulse is assumed to be very short, $R_{\rm NS}/c = 30$ μs. Maximum value of the non-linearity parameter at the location of the particle can reach $\sim 10^3$, but only for sufficiently slow spins $P \geq 100$ ms. If the magnetosphere is modified by the ejected CME to have a monopolar-like structure, the maximal non-linearity parameter that a particle experiences is only few times 10^2. Longer rump-up times will further stretch the curves.

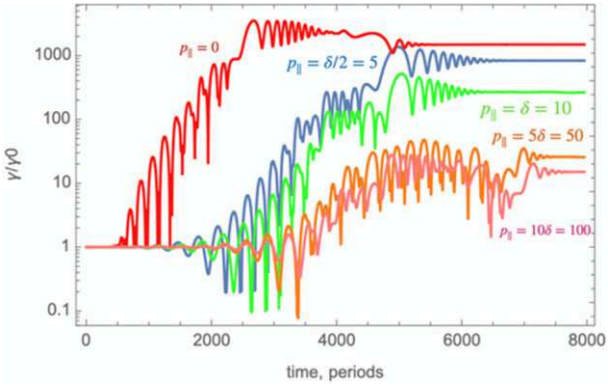

Figure 12 Influence of the initial outward momentum. Evolution of the *relative* Lf of particle moving initially along Bf with various Lfs. Parameters: $\delta = 10$, $f = 100$, $\theta = \pi/4$, $\phi = \pi/4$.

5 EFFECTS OF INITIAL PARALLEL VELOCITY

Opening of the magnetosphere (Section 2.3) will also generate radial plasma outflow. We performed a series of numerical runs that included initial parallel motion of a particle (Fig. 12). Our conclusion is that initial parallel momentum greatly decreases the efficiency of wave–particle interaction.

To estimate the effects of initial parallel momentum, we note that instead of (27) we have

$$\gamma - p_z = \gamma_i - p_i,$$
$$\gamma_i = \sqrt{1 + p_i^2}, \tag{45}$$

where γ_i and p_i are initial Lorentz factor and momentum along the field (away from the direction of pulse propagation), respectively.

We find

$$p_z = \frac{1 + p_0^2/2}{\gamma_i - p_i} - \gamma_i \approx (1 + p_0^2)\gamma_i,$$
$$\gamma = \sqrt{1 + p_0^2 + \frac{\left(1 + p_0^2/2 - \gamma_i^2 + \gamma_i p_i\right)^2}{(\gamma_i - p_i)^2}} \approx (1 + p_0^2)\gamma_i,$$
$$\beta_z = p_z/\gamma \approx 1 - \frac{1}{2(1 + p_0^2)\gamma_i^2},$$
$$\gamma_\parallel \approx \sqrt{(1 + p_0^2)}\gamma_i. \tag{46}$$

The resonant condition (29) now gives, approximately, $\gamma_i \gg 1$,

$$p_0 = \frac{a_0}{1 + \gamma_i^{3/2}/(2\sqrt{2})f} \approx \gamma_i^{-3/2}\frac{a_0}{f}, \tag{47}$$

showing that even mild values of $\gamma_i \sim$ few strongly suppress wave–particle interaction. Qualitatively, initial parallel motion with Lorentz factor γ_i away from the star reduces the initial wave's frequency in the particle frame, leading to higher effective f, and decrease of $\tilde{a}_0$.

6 DISCUSSION

In this work, we consider escape of high-brightness radiation from magnetars' magnetospheres, and conclude that there are multiple ways to avoid non-linear absorption. First, strong non-linear effects are expected in a limited range of parameters, around surface magnetic fields of ~ 10 per cent of critical and spin periods of approximately tens of millisecond. Larger magnetic fields and shorter periods limit the effective non-linearity parameter to $\tilde{a}_0 \leq 10^2$ (see Fig. 2).

In the 'region of interest', we find that ponderomotive acceleration and parallel-adiabatic acceleration of particles are most important. (The magnetospheric structure assumed here assumes a post-CME open magnetosphere.) In a mildly strong leading part of the wave, particles quickly get large parallel momenta – this effectively freezes the interaction. Roughly speaking, in order to obtain transverse momentum $\sim p_0$, a particle needs to surf for time $\sim p_0^2\tau$, where τ is the rump-up time of the electromagnetic pulse. In the inner parts of the magnetosphere, the value of p_0 is suppressed by the guide magnetic field, so a pulse passes through quickly, but does not shake the particles much. Further out, where a stationary particle could have been accelerated to a large Lorentz factor, it never happens because a particle is surfing the pulse and remains at locally low non-linearity parameter, before escaping magnetosphere.

All these issues are further overwhelmed by the parallel large Lorentz factor along the newly opened magnetic field lines, possibly initiated by the opening of the magnetosphere during a CME. Large parallel momentum reduces $\delta = B_w/B_0$ in the particles' frame, and leads to further freezing of the wave–particle dynamics.

We conclude that the case considered by Beloborodov (2021, 2022, 2023), X-mode propagating equatorially across magnetic field, is extreme and is not indicative of the general situation. That is a specific case of no surfing.

ACKNOWLEDGEMENTS

This work had been supported by NASA grants 80NSSC17K0757 and 80NSSC20K0910, and NSF grants 1903332 and 1908590. I would like to thank Alexey Arefiev, Andrei Beloborodov, Pawan Kumar, Mikhail Medvedev, Kavin Tangtartharakul, Chris Thompson, and Bing Zhang for discussions. Publication of this article was funded in part by Purdue University Libraries Open Access Publishing Fund.

DATA AVAILABILITY

The data underlying this article will be shared on reasonable request to the corresponding author.

REFERENCES

Akhiezer A. I., Akhiezer I. A., Polovin R. V., Sitenko A. G., Stepanov K. N., 1975, International Series on Natural Philosophy. Oxford Pergamon Press, p. 1
Beloborodov A. M., 2017, ApJ, 843, L26
Beloborodov A. M., 2021, ApJ, 922, L7
Beloborodov A. M., 2022, Phys. Rev. Lett., 128, 255003
Beloborodov A. M., 2023, preprint (arXiv:2307.12182)
Birdsall C. K., Langdon A. B., 1991, Plasma Physics via Computer Simulation
Bochenek C. D., Ravi V., Belov K. V., Hallinan G., Kocz J., Kulkarni S. R., McKenna D. L., 2020, Nature, 587, 59
Boris J. P., Roberts K. V., 1969, J. Comput. Phys., 4, 552
CHIME/FRB Collaboration, 2020, Nature, 587, 54
Galeev A. A., Sudan R. N., 1989, Basic Plasma Physics. Selected Chapters. Handbook of Plasma Physics, Vols 1 and 2
Golbraikh E., Lyubarsky Y., 2023, ApJ, 957, 102
Goldreich P., Julian W. H., 1969, ApJ, 157, 869
Goldreich P., Julian W. H., 1970, ApJ, 160, 971
Hurley K. et al., 2005, Nature, 434, 1098
Kong L.-B., Liu P.-K., 2007, Phys. Plasmas, 14, 063101
Li C. K. et al., 2021, Nat Astron, 5, 378
Lyubarsky Y., 2014, MNRAS, 442, L9
Lyutikov M., 2003, MNRAS, 346, 540
Lyutikov M., 2022, MNRAS, 509, 2689
Lyutikov M., Popov S., 2020, preprint (arXiv:2005.05093)

Lyutikov M., Rafat M., 2019, preprint (arXiv:1901.03260)
Lyutikov M., Burzawa L., Popov S. B., 2016, MNRAS, 462, 941
Mereghetti S. et al., 2020, ApJ, 898, L29
Metzger B. D., Margalit B., Sironi L., 2019, MNRAS, 485, 4091
Palmer D. M. et al., 2005, Nature, 434, 1107
Popov S. B., Postnov K. A., 2013, preprint (arXiv:1307.4924)
Qu Y., Kumar P., Zhang B., 2022, MNRAS, 515, 2020
Ridnaia A. et al., 2021, Nat. Astron., 5, 372
Roberts C. S., Buchsbaum S. J., 1964, Phys. Rev., 135, 381
Sharma P., Barkov M. V., Lyutikov M., 2023, MNRAS, 524, 6024
Thompson C., 2022, MNRAS, 519, 497
Zeldovich I. B., 1975, Uspekhi Fizicheskikh Nauk, 115, 161

This paper has been typeset from a TEX/LATEX file prepared by the author.